J Mater Sci (2008) 43:7184–7191
DOI 10.1007/s10853-008-3017-z

A facile template-free approach to metal oxide spheres with well-defined nanopore structures

Lingxia Zhang · Chichao Yu · Jianhua Gao · Hangrong Chen · Jianlin Shi

Received: 11 June 2008 / Accepted: 22 September 2008 / Published online: 23 October 2008

Abstract Nanoporous Al_2O_3 with well-defined pore structure, crystallized framework and spherical morphology has been prepared by a facile template-free approach, which involves the preparation via homogeneous precipitation and subsequent decomposition of spherical basic aluminium sulphate particles. The particle size of the spheres can be tuned by controlling the holding time from the beginning of precipitation, and a proper decomposition temperature is important to get high surface area, high pore volume and well-defined pore structures. By the similar way, nanoporous ZrO_2 and TiO_2 spherical particles can also be prepared. These nanoporous oxides all have moderately high surface area (50–70 m^2/g) and well-defined nanopores of around 4–12 nm with very narrow pore size distribution. The frameworks of these oxide spheres consist of many small nanocrystallites, between which the nanopores exist. Compared with the soft and hard template routes, this decomposition strategy of sulphates for nanoporous oxides has the advantages of simplicity and low cost.

Introduction

In the recent years, mesoporous materials with pore size ranging from 2 to 50 nm have been of great interest because of their wide applications in many fields, such as catalysts, sensors, separators and adsorbents [1]. Among them, mesoporous silica materials are most widely studied following the invention of a surfactant-assisted self-assembly route. However, some of non-silica nanoporous materials may have more potential applications in many fields than nanoporous silica. For example, nanoporous Al_2O_3, ZrO_2 and TiO_2 are excellent catalysts to produce fine chemicals, [2–5] and TiO_2 is also very important in environmental catalysis. [4, 5] Nowadays, most of these mesoporous metal oxides are prepared by template strategy, including by using soft templates (surfactants, chelating agents, block copolymers, etc. [6–8]) and/or hard templates (porous anionic alumina, mesoporous silica, polystyrene spheres and carbon nanotubes, etc. [9–12]). In most cases, these two template strategies can only yield nanoporous oxides with pore size smaller than 10 nm or larger than 50 nm, and in some cases, with amorphous framework and poor stability. They are both high cost and the latter one includes multistep synthesis, which would greatly limit their wide applications. Facile synthesis of this kind of nanoporous materials is still a challenge.

As above mentioned, Al_2O_3, TiO_2 and ZrO_2 powders are widely applied to produce catalysts, [4, 5] ceramics, [13] adsorbents and chromatographic columns, etc. On the other hand, the effective control over their particle shapes, crystallite sizes and pore structures is still a great task for researchers. Commonly, decomposition of hydroxides or salts in an air atmosphere could lead to the formation of corresponding oxide powders. However, these powders are usually randomly packed with irregular morphologies composed of fine (nano- or micro-sized) particles without significant pore structures. If the metal hydroxides/salts could be synthesized with controlled morphologies, e.g. spherical particles, a careful decomposition may retain the

L. Zhang · C. Yu · J. Gao · H. Chen · J. Shi (✉)
State Key Lab of High Performance and Superfine Microstructure, Shanghai Insitute of Ceramics, Chinese Academy of Science, 1295 Ding-xi Road, Shanghai 200050, People's Republic of China
e-mail: jlshi@sunm.shcnc.ac.cn

L. Zhang
e-mail: zhlingxia@mail.sic.ac.cn

original morphologies of the hydroxides/salts and pores can be generated during the decomposition process. Homogeneous precipitation has been used to prepare aluminium, titanium, zirconium, ferric and gallium hydroxide nanoparticles using urea, which can slowly decompose and give out OH^- in solution during heating and make the pH value of solutions increase slowly and homogeneously [13–24]. No doubt, a route of decomposing these hydroxides into nanoporous oxide particles, if possible, will be simple and low cost in comparison with the template methods. In this report, nanoporous Al_2O_3, ZrO_2 and TiO_2 materials with well-defined pore size distribution (PSD) and spherical morphology are prepared simply by thermal decomposition of metal basic sulphate spheres, which were fabricated with a homogeneous precipitation method. Physicochemical properties, such as particle morphologies, pore structures, surface area, pore volume and diameter of these metal oxides calcined at different temperatures are characterized.

Experimental

Materials

The starting materials were analytical grade $CO(H_2N)_2$ (≥99.0%), $NH_4Al(SO_4)_2 \cdot 12H_2O$(≥99.5%), $Zr(SO4)_2 \cdot 4H_2O$(≥98.0%) and chemical grade $Ti(SO_4)_2$(≥96.0%). All reagents are purchased from Sinopharm Chemical Reagent Co., LtdS (SCRC) of China and used without further purification.

Nanoporous Al_2O_3

For the preparation of aluminium hydroxide, 50 g $CO(H_2N)_2$ and 18 g $NH_4Al(SO_4)_2 \cdot 12H_2O$ were added to 200 mL H_2O, respectively. These two transparent solutions were then mixed at 80 °C water bath under stirring. The occurrence of precipitation can be clearly observed in the glass bottle. After a hold time (t_h) of 3, 8, 18, 25, 40, 60 min since the initiation of precipitation, the precipitated solution was immediately cooled down under flowing water to room temperature. Then the powder was filtered out and washed repeatedly by H_2O. After drying at 100 °C for 2 days, the powder was calcined at 950, 1000, 1050, 1100, 1150 °C, respectively, for 2 h with a heating rate of 3 °C/min.

Nanoporous TiO_2

$Ti(SO_4)_2$ (9.6 g) and $CO(H_2N)_2$ (100 g) were dissolved in 600 and 400 mL H_2O, respectively. These two transparent solutions were then mixed at 80 °C water bath under stirring. The hold time since the mixture of these two solutions was 5 h. The powder sample was directly filtered out and washed repeatedly by H_2O. Then it was dried at 100 °C for 2 days and calcined at 450, 500, 550, 600 °C, respectively, for 2 h with a heating rate of 3 °C/min.

Nanoporous ZrO_2

$ZrSO_4$ (7.11 g) and $CO(H_2N)_2$ (120 g) were dissolved in 250 and 120 mL H_2O, respectively. These two transparent solutions were then mixed at 80 °C water bath under stirring and precipitation formed immediately. After 15 min, the powder sample was directly filtered out and washed repeatedly by H_2O. Then it was dried at 100 °C for 2 days and calcined at 600, 650, 700, 750, 800 °C, respectively, for 2 h with a heating rate of 3 °C/min.

Characterization

XRD (X-ray diffraction) patterns were recorded on a Rigaku D/Max 2200PC diffractometer using Cu Ka radiation at 40 kV and 40 mA. Nitrogen adsorption-desorption isotherms at 77 K were measured on a Micromeritics TriStar 3000 instrument. All samples were outgassed at 200 °C for 12 h under flowing helium before measurements. The specific surface areas were calculated with the BET (Brunauer–Emmet–Teller) methods. Pore size and PSD plots were obtained by BJH (Barrett–Joyner–Halenda) method using the cylindrical pore model. FETEM (field emission transmission electron microscopy) analysis was conducted with a JEOL 200CX electron microscope operated at 200 KeV. FE-SEM (field emission scanning electron microscopy) analysis was performed on a JEOL JSM6700F electron microscope. TG-DTA measurements were conducted using a NETZSCH STA 449C apparatus with an air flow of 20 mL/min and a heating rate of 10 °C/min.

Results and discussion

Nanoporous Al_2O_3

The as-synthesized aluminium hydroxide is amorphous, as can be seen in Fig. 1 pattern a. Chemical analysis shows that there is 27.79 wt% of SO_4^{2-} incorporated into the aluminium hydroxide, which indicates that the precipitate is basic aluminium sulphate [14, 15]. After calcination at certain temperatures, aluminium hydroxide decomposes. In Fig. 2, the endothermal peaks at 900 and 927 °C in the DTA curve of the precipitate indicate the decomposition of SO_4^{2-}. The transformation of γ-Al_2O_3 to α-Al_2O_3 gives a exothermal peak at 1,200 °C. Generally, aluminium hydroxide does not exist in the form of spherical particles. The incorporation of SO_4^{2-} into the precipitate makes the aluminium hydroxide particles have spherical morphology.

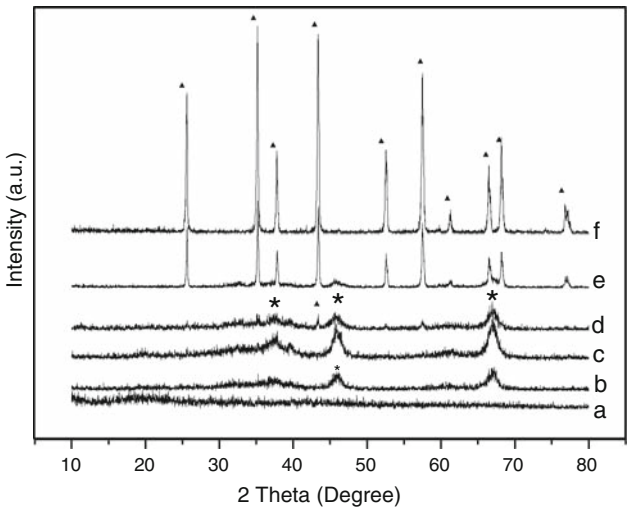

Fig. 1 XRD patterns of **a** the as-synthesized aluminium hydroxide precipitate and the samples calcined at **b** 950 °C, **c** 1,000 °C, **d** 1,050 °C, **e** 1,100 °C, **f** 1,150 °C (▲: α-Al_2O_3; *: γ-Al_2O_3)

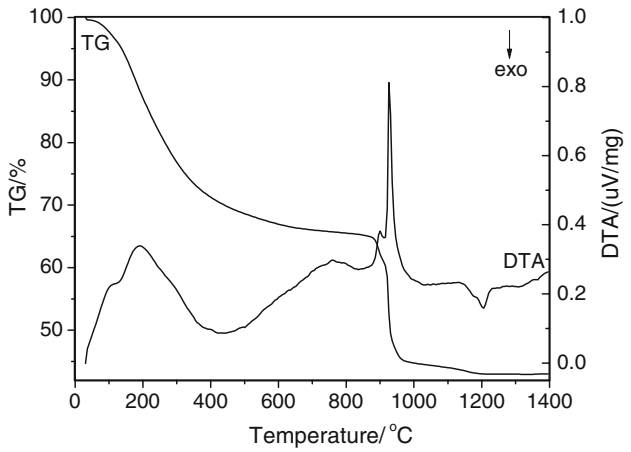

Fig. 2 Thermal behaviour of aluminium hydroxide precipitate

Figure 3 shows the precipitate particles at various hold times (t_h). It can be seen that the particles are spherical and grow from 400 to 600 nm when t_h increases from 3 to 25 min. These spherical particles become more agglomerate with longer precipitation time. After 25 min, many smaller particles were obtained because of the second burst of nucleation and the size of particles becomes widely distributed [14, 15]. Therefore, when t_h is within 25 min, the size of the precipitate particles can be slightly tuned by controlling t_h and spherical particles with rather uniform size can be obtained.

As an example, the precipitate at $t_h = 3$ min has been calcined. Figure 1 shows the XRD patterns of Al_2O_3 obtained at different calcination temperatures. As commonly known, when the calcination is conducted below 1000°C, aluminium hydroxide decomposes to γ-Al_2O_3, which shows three wide peaks at about $2\theta = 67°$, 46° and 37°. These three peaks almost disappear after calcination at 1,100 °C, and meanwhile, α-Al_2O_3 forms at above 1,050 °C, as indicated by the peak at about $2\theta = 43°$. With the increase of calcination temperature, many diffraction peaks with high intensity, corresponding to pure α-Al_2O_3, can be observed.

N_2 adsorption-desorption isotherms and BJH desorption PSD plots of Al_2O_3 calcined at different temperatures are shown in Fig. 4, and their corresponding pore structural parameters are summarized in Table 1. A rather high BET specific surface area of about 58 m^2/g can be obtained when the precipitates were calcined at 1,050 °C. The typical irreversible type IV adsorption–desorption isotherms with a H1 hysteresis loop indicate its well-defined worm-like mesoporous structure and narrow PSD. The adsorption inflection at the relative pressure from 0.8 to 1.0 is associated with capillary condensation taking place in the mesopores and its steepness reveals the uniformity of mesopore size. As shown in BJH desorption pore diameter

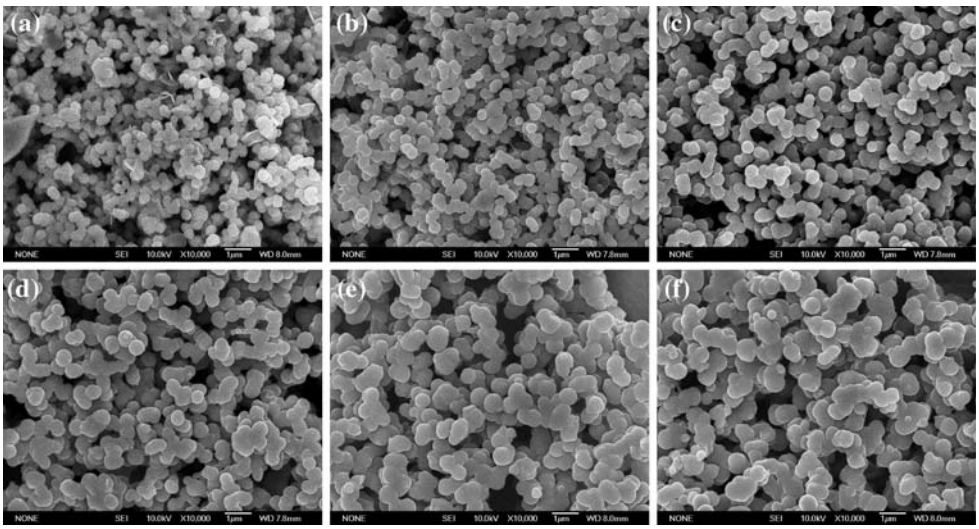

Fig. 3 SEM images of the aluminium hydroxide precipitates at different t_h: **a** 3 min, **b** 8 min, **c** 18 min, **d** 25 min, **e** 40 min and **f** 60 min

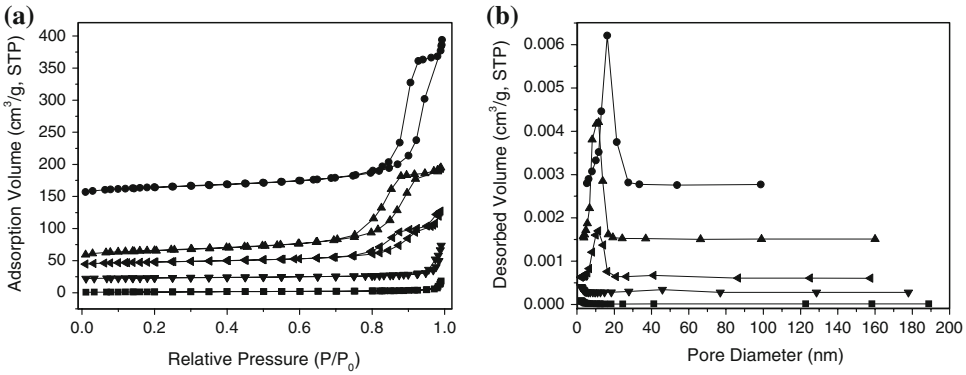

Fig. 4 **a** N_2 adsorption–desorption isotherms and **b** BJH desorption PSD plots of Al_2O_3 calcined at (■) 950 °C, (▼) 1,150 °C, (◀) 1,100 °C, (▲) 1,050 °C, (●) 1,000 °C

Table 1 Pore structural parameters of Al_2O_3 calcined at different temperatures

Calcined temperature (°C)	S_{BET} ($m^2\ g^{-1}$)	V_{BJH} ($cm^3\ g^{-1}$)	D_{BJH} (nm)
950	4.5	0.03	–
1,000	55	0.38	19
1,050	58	0.23	11.5
1,100	28	0.14	15
1,150	10	0.07	–

S_{BET} BET surface area, V_{BJH}, D_{BJH} BJH desorption average pore volume and diameter

distribution patterns in Fig. 4b, the pore size of the sample calcined at 1,050 °C is centred at 11.5 nm. The pore volume and the surface area decrease when the precipitates were calcined above this temperature. No obvious peaks in the PSD patterns and no inflection in BET isotherms can be found when the calcination was conducted at temperature <950 °C, or >1,150 °C, which indicates that almost no pores have been produced under these calcination conditions. At 950 °C and lower temperature, the aluminium hydroxide cannot decompose completely, pore channels have not opened and thus the pore volume and the surface area of Al_2O_3 are very low. As for the sample calcined at above 1100°C, the formation and afterwards crystallite growth of α-Al_2O_3 phase, together with the interparticle sintering and closing of the mesopores, result in the dramatically decrease of their pore volume and surface area. Existence of γ-Al_2O_3 phase is important to get high surface area. Lanthanum has been used to modify γ-Al_2O_3 prepared by homogeneous precipitation. Thus, the γ-Al_2O_3 can be stable up to 1,300 °C [18]. Further studies on how to increase the surface area of these nanoporous Al_2O_3 are in progress.

Figure 5 gives the SEM and TEM images of Al_2O_3 calcined at 1,000 °C. It can be seen that the Al_2O_3 nanoparticles are still spherical. However, the particles are frangible and a part of them have been broken to chippings at high temperature. The sphere surface is no longer as smooth as can be found in Fig. 3 for powders before decomposition and these spheres are loosely packed with many ultrafine nanocrystallites of γ-Al_2O_3. Wormlike mesopores between these nanocrystallites can be observed in TEM images. With the increase of calcination temperature, these γ-Al_2O_3 nanocrystallites transform to α-Al_2O_3 with a very quick crystallite growth. This phase transformation results in the decrease of surface area and pore volume, as can be concluded from their above N_2 sorption and XRD analysis. As a comparison, commercial aluminium sulphate has been calcined directly at 1,100 °C and irregularly shaped Al_2O_3 particles of larger than 10 μm in

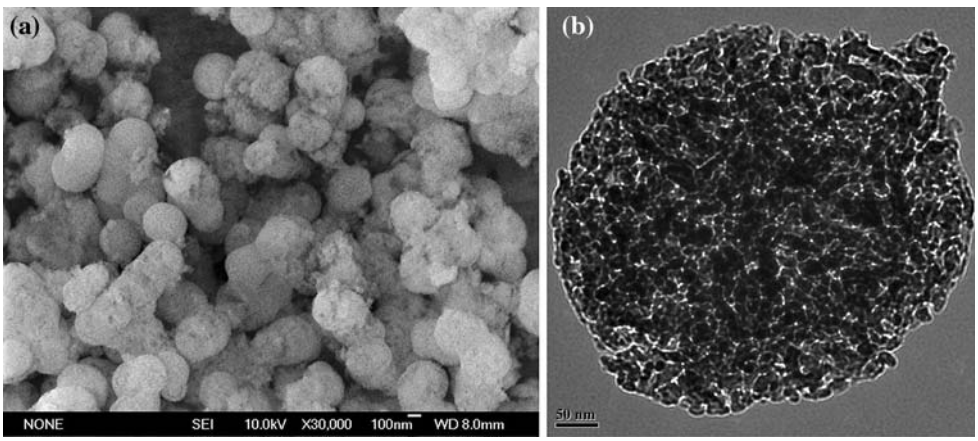

Fig. 5 **a** SEM and **b** TEM images of the Al_2O_3 particles calcined at 1,000 °C

size were obtained, which are composed of many small gathered nanoparticles. Thus, this homogeneous precipitation process is helpful to synthesize uniform and fine nanoporous Al_2O_3 particles.

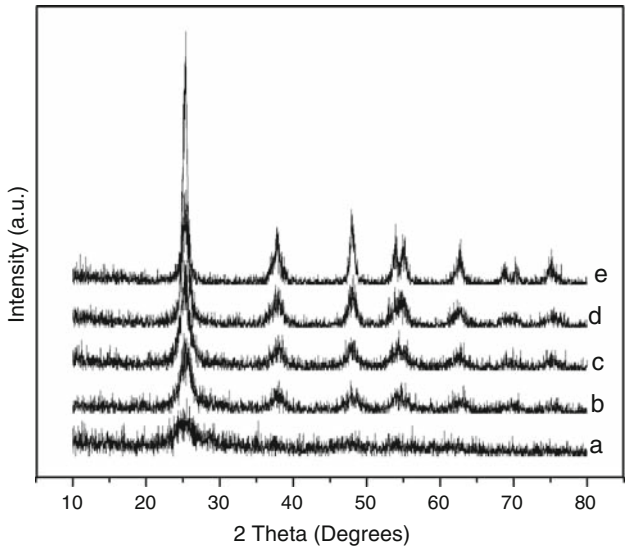

Fig. 6 XRD spectra of **a** the as-synthesized titanium hydroxide precipitate and TiO_2 calcined at **b** 450 °C, **c** 500 °C, **d** 550 °C, **e** 600 °C

Nanoporous TiO_2

Homogeneous precipitation is the most effective method to produce TiO_2 powders as photocatalysts [19–21]. Basic titanium sulphate precipitate has also been prepared by homogeneous precipitation using urea. The as-synthesized precipitate is also amorphous (Fig. 6 pattern a). Figure 6 also shows the XRD patterns of TiO_2 calcined at different temperatures. After calcination at 450–600 °C, the precipitate decomposes to TiO_2. All the diffraction peaks are in good agreement with anatase TiO_2, which have shown much better photocatalytical properties than rutile TiO_2 [4, 5]. The obvious broadening of the diffraction peaks is ascribed to the small size of the TiO_2 nanocrystallites. The diffraction peaks of anatase TiO_2 became intensive as the calcination temperature was raised to 600 °C, which indicated the formation of large crystallites.

The particle morphology and the porous structure of TiO_2 calcined at 500 °C were investigated by SEM and TEM, as shown in Fig. 7. Spherical particles, which slightly agglomerate with each other, can be observed. SEM image of the particles shows that the particle surface has many small protuberances, which are small TiO_2 created during the second nucleation. Further details can be found in the TEM image. The spherical particles of TiO_2

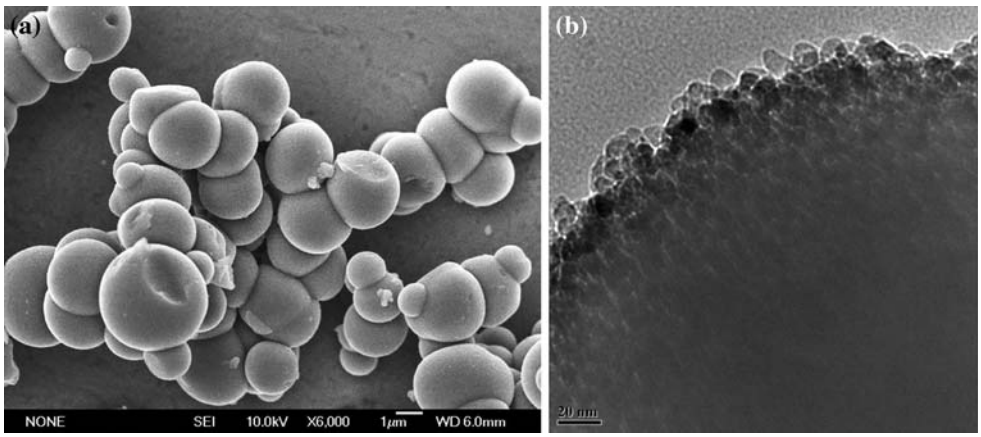

Fig. 7 **a** SEM and **b** TEM images of TiO_2 particles calcined at 550 °C

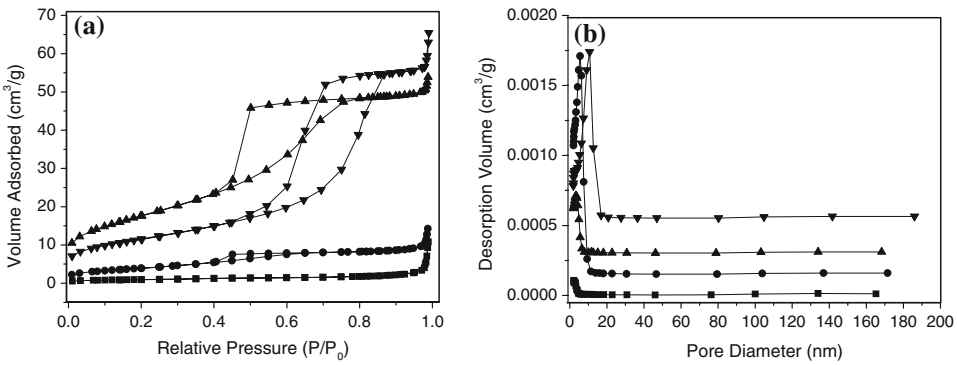

Fig. 8 **a** N_2 adsorption–desorption isotherms and **b** BJH adsorption PSD plots of TiO_2 calcined at (■) 450 °C, (●) 500 °C, (▲) 550 °C, (▼) 600 °C

are the aggregates of numerous nanocrystallites and wormlike nanopores between these nanocrystallites can be observed, which are similar to the case of Al_2O_3.

Figure 8 gives the N_2 adsorption-desorption isotherms and BJH adsorption PSD plots of TiO_2 calcined at different temperatures. Their corresponding pore structural parameters are summarized in Table 2. The highest BET surface area of about 64 m^2/g can be obtained when the precipitate was calcined at 550 °C. The irreversible type IV adsorption-desorption isotherms with a H1 hysteresis loop also indicate their well-defined wormlike mesoporous feature. The PSD is extremely narrow and centres at about 5.0 nm. The decrease of surface area of TiO_2, which arises from the incomplete decomposition of the precipitate at low temperatures (<500 °C) and the growth of crystals at high temperatures (>600 °C), can also be observed. No pores or lower pore volume have been obtained at 450 °C because of the non-decomposition of the precipitate, as can be concluded from the N_2 isotherms and PSD plots.

Table 2 Pore structural parameters of TiO_2 calcined at different temperatures

Calcined temperature (°C)	S_{BET} (m^2 g^{-1})	V_{BJH} (cm^3 g^{-1})	D_{BJH} (nm)
450	3.5	0.017	–
500	14	0.023	5.8
550	64	0.087	4.9
600	42	0.10	8.7

S_{BET} BET surface area, V_{BJH}, D_{BJH} BJH adsorption average pore volume and diameter

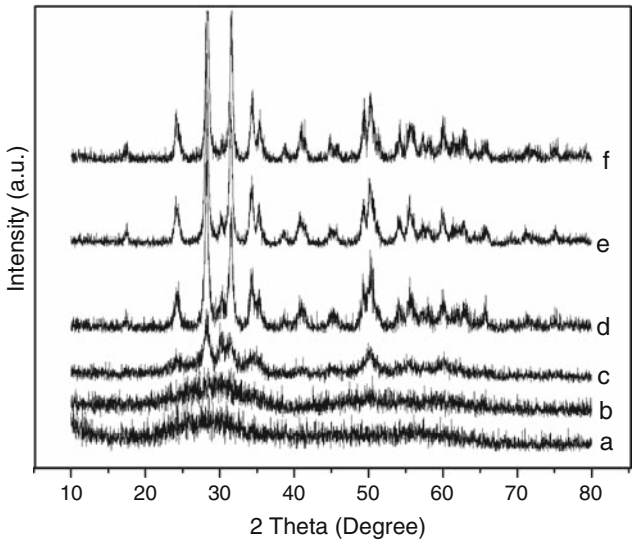

Fig. 9 XRD spectra of (a) the as-synthesized zirconium hydroxide precipitate and ZrO_2 calcined at (b) 600 °C, (c) 650 °C, (d) 700 °C (e) 750 °C and (f) 800 °C

Nanoporous ZrO_2

Basic titanium sulphate precipitate has also been synthesized using the same method. The XRD patterns of ZrO_2 calcined at different temperatures are shown in Fig. 9. The as-synthesized precipitate is also amorphous (Fig. 9 pattern a). The decomposition of SO_4^{2-} does not take place below 600 °C and the powder is still amorphous (Fig. 9 pattern b). With the increase of calcination temperature, intensive diffraction peaks, which are in good agreement with tetragonal ZrO_2, can be observed. SEM and TEM images of ZrO_2 particles after calcination at 700 °C are shown in Fig. 10. These ZrO_2 particles also have spherical morphology and the same porous structure as Al_2O_3 and TiO_2.

N_2 adsorption–desorption isotherms and the BJH desorption PSD plots of ZrO_2 calcined at different temperatures are shown in Fig. 11. Their mesoporous nature is proved by the irreversible type IV adsorption-desorption isotherms with a H1 hysteresis loop. When the precipitate was calcined at 700 °C, their BET surface area reached a maximum value of about 69 m^2/g and their average pore diameter is 5.3 nm (Table 3). At the same time, it also has very narrow PSD. The same decrease of surface area at

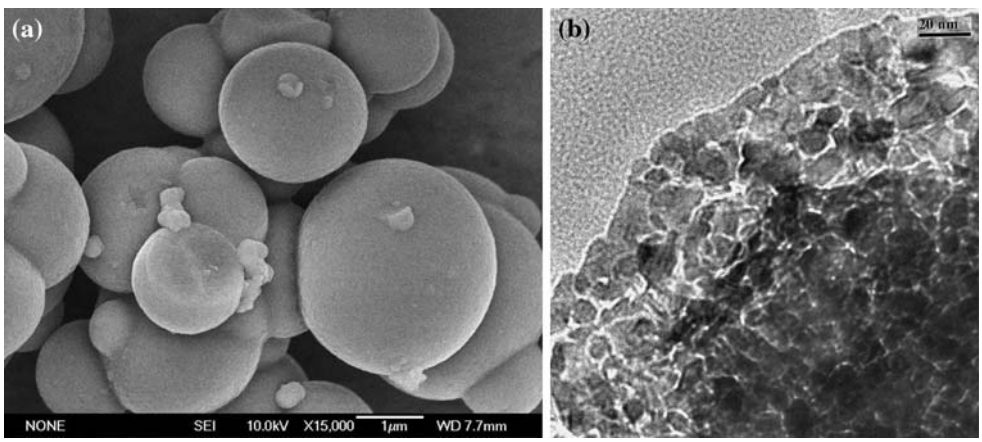

Fig. 10 **a** SEM and **b** TEM images of ZrO_2 particles calcined at 700 °C

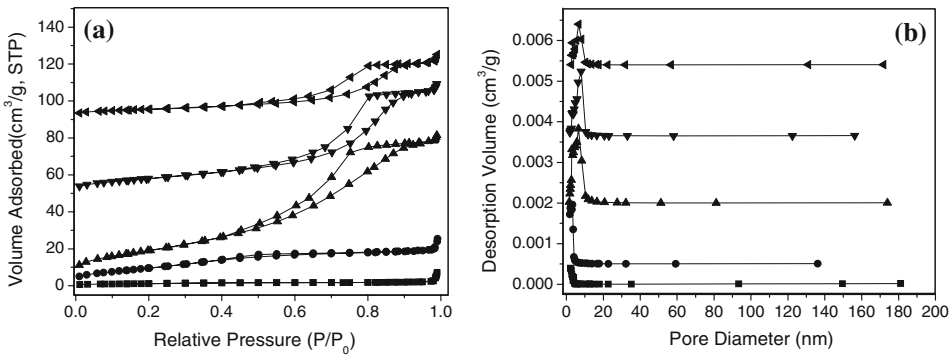

Fig. 11 **a** N_2 adsorption–desorption isotherms and **b** BJH desorption PSD plots of ZrO_2 calcined at (■) 600 °C, (●) 650 °C, (▲) 700 °C, (▼) 750 °C and (◀) 800 °C

Table 3 Pore structural parameters of ZrO_2 calcined at different temperatures

Calcined temperature (°C)	S_{BET} ($m^2\ g^{-1}$)	V_{BJH} ($cm^3\ g^{-1}$)	D_{BJH} (nm)
600	4.4	0.01	–
650	36	0.04	7.4
700	69	0.13	5.3
750	40	0.10	7.0
800	20	0.06	7.6

S_{BET} BET surface area, V_{BJH}, D_{BJH} BJH desorption average pore volume and diameter

temperatures lower than 600 °C and higher than 800 °C has also been observed and can be attributed to the same reasons as those for TiO_2.

Conclusion

A facile template-free approach has been developed for the preparation of mesoporous metal oxides. In this approach, spherical basic aluminium sulphate particles, for example, were prepared by a homogeneous precipitation method using urea. These particles grow from 400 to 600 nm when precipitation time increased from 3 to 25 min. The size of particles becomes more widely distributed after 25 min because of the second burst of nucleation and particle agglomeration. Decomposition of these basic sulphates at a moderate temperature in air results in mesoporous Al_2O_3 spherical particles with very narrow PSD at around 11.5 nm and moderately high surface area (58 m^2/g). Effects of different calcination temperatures on their surface areas and pore sizes have been studied. Their surface areas and pore volumes show decreases at either overlow or overhigh calcination temperatures, which could be attributed to the incomplete decomposition of the basic sulphates at overlow temperatures and the extensive crystallite growth of the oxides at overhigh temperatures, respectively. With the similar approach, Mesoporous tetragonal zirconia and anatase titania were also obtained. They also have spherical particles, crystallized framework and show well-defined pore structure, narrow PSD at around 5 nm and moderately high surface area (>60 m^2/g). This strategy, which is based on a simple decomposition of basic metal sulphate powders prepared by homogeneous precipitation, presents a facile, low-cost and effective process to synthesize nanoporous metal oxides.

Acknowledgements The authors gratefully acknowledge the financial supports from the National Science Foundation of China (Grant No. 50702072, 20703055, 20633090), the Shanghai Rising Star Project (Grant No. 08QA14074).

References

1. Shi JL, Hua ZL, Zhang LX (2004) J Mater Chem 5:795
2. Chen HR, Shi JL, Li YS, Yan JN, Hua ZL, Chen HG, Yan DS (2003) Adv Mater 15:1078
3. Yin DH, Qin LS, Liu HF (2005) J Mol Catal A Chem 240:40
4. Sun J, Gao L, Zhang QH (2003) J Am Ceram Soc 86:1677
5. Bakardjieva S, Šubrt J, Štengl V, Dianez MJ, Sayagues MJ (2005) Appl Catal B Environ 58:193
6. Kresge CT, Leonowicz ME, Roth WJ, Vartuli JC, Beck JS (1992) Nature 359:710
7. Yang P, Zhao DY, Margolese DI, Chmelka BF, Stucky GD (1998) Nature 396:152
8. Zhao DY, Feng JL, Huo QS, Melosh N, Fredrickson GH, Chmelka BF, Stucky GD (1998) Science 279:548
9. Ryoo R, Joo SH, Kruk M, Jaroniec M (2001) Adv Mater 13:677
10. Ying JY, Mehnert CP, Wong MS (1999) Angew Chem Int Ed 38:56
11. Tian BZ, Liu XY, Yang HF, Xie SH, Yu CZ, Tu B, Zhao DY (2003) Adv Mater 15:1370
12. Tian BZ, Liu XY, Tu B, Yu CZ, Fan J, Wang LM, Xie SH, Stucky GD, Zhao DY (2003) Nature Mater 2:159
13. Shi JL, Gao JH (1995) J Mater Sci 30:793
14. Shi JL, Gao JH, Lin ZX (1989) Solid State Ion 32–33:537
15. Shi JL, Gao JH, Ruan ML (1992) Chin J Inorg Chem 7:161
16. Adachi-Pagano M, Forano C, Besse JP (2003) J Mater Chem 13:1988
17. Ada K, Sarikaya Y, Alemdaroglu T, Onal M (2003) Ceram Int 29:513
18. Ozawa M, Nishio Y (2004) J Alloy Compd 374:397
19. Ookubo A, Ooi K, Tomita T (1989) J Mater Sci 24:3599

20. Zanella R, Giorgio S, Henry CR, Louis C (2002) J Phys Chem B 106:7634
21. Seo DS, Kim H, Jung HC (2003) J Mater Res 18:571
22. Tas AC, Majewski PJ, Aldinger F (2002) J Am Ceram Soc 85:1421
23. Bakardjieva S, Šubrt J, Štengl V, Vecernikova E, Bezdicka P (2003) Solid State Phenom 90–91:7
24. Šubrt J, Boháček J, Štengl V, Grygar T, Bezdička P (1999) Mater Res Bull 34:905